AIP | Applied Physics Letters

Measurement of the indium concentration in high indium content InGaN layers by scanning transmission electron microscopy and atom probe tomography

T. Mehrtens, M. Schowalter, D. Tytko, P. Choi, D. Raabe, L. Hoffmann, H. Jönen, U. Rossow, A. Hangleiter, and A. Rosenauer

Citation: Applied Physics Letters **102**, 132112 (2013); doi: 10.1063/1.4799382
View online: http://dx.doi.org/10.1063/1.4799382
View Table of Contents: http://scitation.aip.org/content/aip/journal/apl/102/13?ver=pdfcov
Published by the AIP Publishing

Measurement of the indium concentration in high indium content InGaN layers by scanning transmission electron microscopy and atom probe tomography

T. Mehrtens,[1,a)] M. Schowalter,[1] D. Tytko,[2] P. Choi,[2] D. Raabe,[2] L. Hoffmann,[3] H. Jönen,[3] U. Rossow,[3] A. Hangleiter,[3] and A. Rosenauer[1]
[1]*Insitut für Festkörperphysik, Universität Bremen, Otto-Hahn-Allee 1, D-28359 Bremen, Germany*
[2]*Max-Planck-Institut für Eisenforschung GmbH, Max-Planck-Str. 1, D-40237 Düsseldorf, Germany*
[3]*Insitut für Angewandte Physik, TU Braunschweig, Mendelssohnstr. 2, D-38106 Braunschweig, Germany*

(Received 18 February 2013; accepted 20 March 2013; published online 4 April 2013)

A method for determining concentrations from high-angle annular dark field-scanning transmission electron microscopy images is presented. The method is applied to an InGaN/GaN multi-quantum well structure with high In content, as used for the fabrication of light emitting diodes and laser diodes emitting in the green spectral range. Information on specimen thickness and In concentration is extracted by comparison with multislice calculations. Resulting concentration profiles are in good agreement with a comparative atom probe tomography analysis. Indium concentrations in the quantum wells ranging from 26 at. % to 33 at. % are measured in both cases. [http://dx.doi.org/10.1063/1.4799382]

For the development of opto-electronic based devices such as portable projection systems, direct emitting green laser diodes are of large interest. InGaN with its bandgap ranging from 3.507 eV (GaN)[1] to 0.7 eV (InN)[2] is currently the most promising material for this purpose. For an emission wavelength of >500 nm, an In concentration of >26 at. % is needed.[3] Furthermore, In has to be homogeneously incorporated and quantum wells of this material must possess a low density of non-radiative defects for lasing.

For materials such as InGaAs, transmission electron microscopy (TEM) methods such as strain state analysis can be applied to study the layer homogeneity and concentration,[4] but this method is problematic for InGaN due to electron beam induced damage which can be falsely interpreted as compositional inhomogeneities.[5] Rosenauer *et al.*[6] recently showed that for high-angle annular dark field-scanning transmission electron microscopy (HAADF-STEM), electron beam induced damage can be largely suppressed under conventional imaging conditions at 300 keV due to the lower electron dose exposed on the specimen.

In this letter, we demonstrate the method of Rosenauer *et al.*[6,7] for composition analysis from HAADF-STEM images on InGaN layers with high In content (>25 at. %) and compare the results with an atom probe tomography (APT) study. The investigated specimen was a five-fold InGaN multi-quantum well structure grown by metal-organic vapour phase epitaxy (MOVPE) in a horizontal reactor (Aixtron AIX 200RF). The quantum wells had a thickness of ≈1.7 nm and were separated by 20 nm GaN barriers. The growth temperature of the quantum wells was 700 °C (for more details on specimen growth, we refer to Hoffmann *et al.*[8]). For HAADF-STEM analysis, a thin lamella was prepared using the common lift-out technique.[9] To reduce preparation induced amorphous surface layers, subsequent low-energy ion milling at 400 eV was applied using a Gentle Mill.[10] For APT measurements, needle-shaped specimens were prepared also by FIB milling using the lift-out method as described in Thompson *et al.*[11] For sharpening the blanks to APT tips, annular FIB milling was applied where the energy of the ions was reduced in the last steps to 5 keV and finally 2 keV to minimize the amount of implanted Ga ions. HAADF-STEM images were recorded using a FEI Titan 80/300 equipped with an HAADF-detector (FischioneModel 3000) at an acceleration voltage of 300 keV. Atom probe tomography was conducted using an Imago LEAP™ 3000X HR system.

The basic idea of composition analysis by HAADF-STEM is a comparison of measured image intensities with reference data. The reference data were calculated by multislice simulations in the frozen lattice approach using the STEMSIM software.[12] Simulations were carried out for In concentrations ranging from 0 to 55 at. % in steps of 5% with the electron beam parallel to the $[11\bar{2}0]$-direction. For each simulation, a crystal supercell of 6 × 6 unit cells in [0001] and $[1\bar{1}00]$ directions and 150 nm in electron beam direction was generated. To consider static atomic displacements[13] due to different covalent radii of Ga and In, the overall force in the supercell was minimized using a Stillinger-Weber[14] potential implemented into the LAMMPS-code.[15] Afterwards, all atoms were statistically displaced from their equilibrium positions according to their Debye-Waller factors. In our case, a set of Debye-Waller factors from density-functional theory calculations were used.[16] For a more detailed description of the simulations, we refer to the publications of Rosenauer *et al.*[6,7] The intensity scattered to angles between 10 mrad and 350 mrad was circularly averaged over small annuli lying within this region and stored in dependence of the specimen thickness in steps of 1 nm. All values are normalized to the intensity of the incident electron beam. In Fig. 1(a), the radial intensity distribution is shown for GaN and $In_{0.3}Ga_{0.7}N$ at a specimen thickness of 100 nm. In recent publications,[6,7,17] it was demonstrated that the

a)Electronic mail: mehrtens@ifp.uni-bremen.de

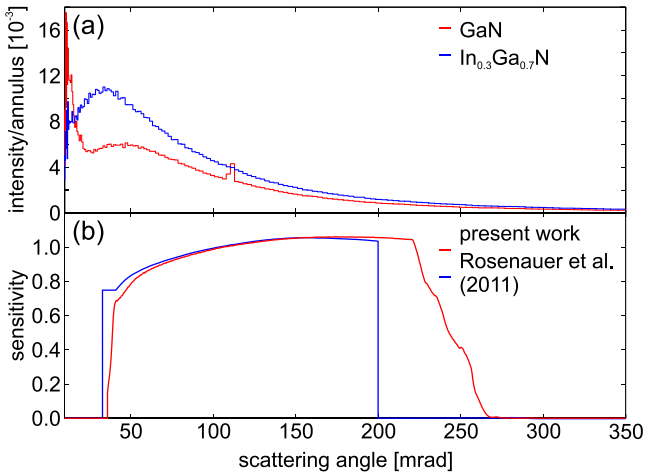

FIG. 1. Simulated radial intensity distribution of GaN and $In_{0.3}Ga_{0.7}N$ for a specimen thickness of 100 nm (a). Radial detector sensitivity of Rosenauer *et al.* (see Ref. 6) and sensitivity used in this work (b).

HAADF detector shows a non-uniform detection sensitivity. Thus, simulated data have to be corrected[7,18] for accurate quantification. In our case, the simulations are corrected by weighting the radially stored intensity according to the radial sensitivity of the HAADF detector for the used camera length of 196 mm. The sensitivity is measured by scanning the electron probe over the detector resulting in a detector scan as shown in Fig. 2(a). For the present study, it was necessary to refine the sensitivity curve published by Rosenauer *et al.*[6] (see Fig. 1(b)) because the approximations used in this work led to an underestimation of In-concentrations of approximately 5 at. % at $x = 0.3$. Three improvements have been made. Foremost, the inner detector angle changed from 33 mrad to 36 mrad. This is caused by the fact that the value of 33 mrad has been measured from a shadow image of the detector, but the projected inner radius deviates from the actual inner radius due to projection effects.[17] Second, the plateau between 33 mrad and 41 mrad is not present anymore. Rosenauer *et al.*[6] assumed that the inner detector rim depicted in Fig. 2(b) appears broadened due to the lateral extension of the scanning electron probe. This would mean that a convolution of the probe and the detector and

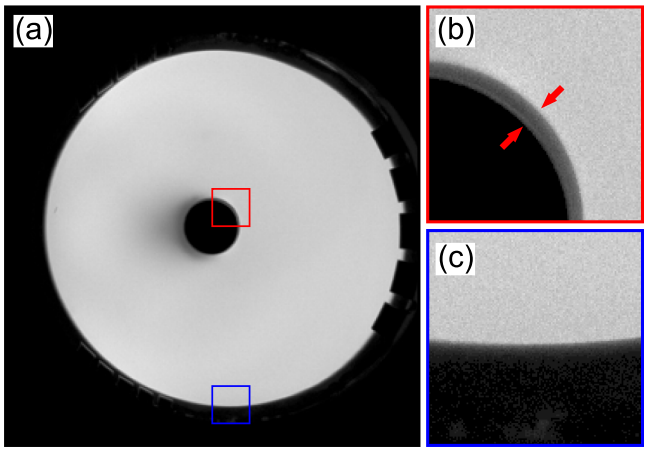

FIG. 2. HAADF detector (a), broadened inner detector rim indicated by red arrows (b), and outer detector rim (c) (all images are gamma enhanced for better visibility).

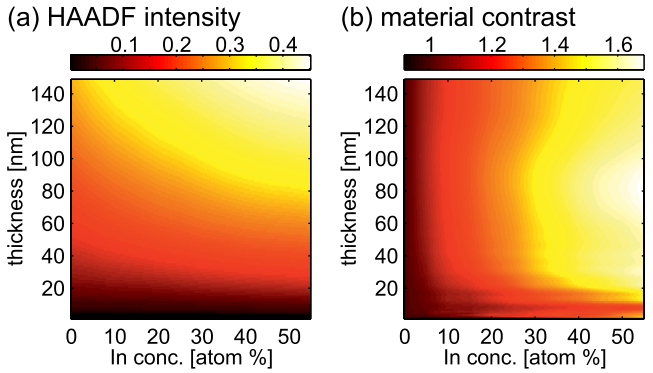

FIG. 3. Simulated reference data (a) and simulated material contrast (b).

neighboring vacuum is measured at the rim. In this case, the outer detector rim should also appear broadened, but Fig. 2(c) shows a sharp border between the detector and vacuum. Hence, the slowly decreasing sensitivity at the inner rim is a real detector feature and must be considered. Finally, the sensitivity curve now includes scattering angles up to 270 mrad in contrast to the curve of Rosenauer *et al.*, which was truncated at 200 mrad.

The results of the simulation (weighted by the sensitivity curve starting at 36 mrad) are shown in Fig. 3(a) for varying specimen thicknesses and In concentrations (for a parameterization of simulated data see supplemental material).[22] The intensity is increasing with increasing specimen thickness as well as with increasing In content (Z-contrast). In Fig. 3(b), the resulting material contrast (ratio of InGaN and GaN intensity) is shown. A maximum contrast of 1.68 for an In concentration of 50 at. % can be seen for a specimen thickness of 80 nm.

Fig. 4(a) shows a high resolution HAADF-STEM image of one InGaN layer (QW1). The growth direction in this

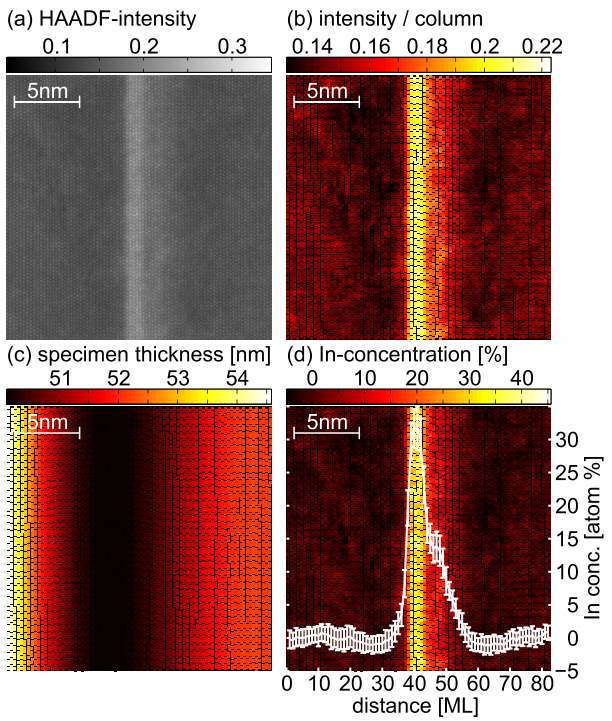

FIG. 4. HAADF-STEM image of an InGaN layer (a), average intensity per atomic column (b), specimen thickness (c), and concentration map and according concentration profile (d).

image (and all following images) runs from the left to the right side of the image.

To allow a comparison between simulated and experimental data, measured intensities are normalized with respect to the intensity of the scanning electron probe. The intensity of the probe is measured from the detector scan of Fig. 2(a).[7,17] In the following step, the mean intensity per atomic column shown in Fig. 4(b) is calculated by subdividing the image into Voronoi-cells.[6] A Voronoi cell of an atomic column is the cell formed by the perpendicular bisectors of the direct connections to the neighboring columns. The specimen thickness is shown in Fig. 4(c). It is derived from the intensity per atomic column measured in the GaN barriers surrounding the InGaN layer by comparison with the according reference data for GaN from Fig. 3(a). For the InGaN layer, specimen thickness and In concentration are unknown, but either of these two values has to be known to evaluate the other. Thus, the specimen thickness derived from the neighboring GaN is interpolated over the InGaN layer using a polynomial fit. Afterwards, for each atomic column located in the InGaN layer, its intensity is compared with the reference data in Fig. 3(a) taking the interpolated specimen thickness into account. Fig. 4(d) shows the final concentration map and the concentration profile deduced by averaging along single monolayers (MLs). At the central monolayer of the InGaN layer, a concentration of (31.8 ± 3.2) at. % In is measured. It can also be seen that diffusion of In into the GaN barrier occured during growth, resulting in an additional InGaN layer of around 14 at. % In.

In a comparative study, the specimen was also investigated by APT. The measurement conditions were optimized by cooling the specimen to a temperature of 40 K and reducing the laser pulse energy to 0.05 nJ at a frequency of 100 kHz. As a result, an average III:V-ratio of 53:47 was measured which only slightly deviates from the expected 50:50-ratio. The measured nitrogen deficiency could originate from multiple ion impacts on the position-sensitive detector. De Geuser *et al.*[19] proposed that field evaporation of an atom from an APT specimen may increase the evaporation field of neighboring atoms, leading to successive field evaporation of atoms (termed as correlated field evaporation) and to multiple ion impacts on the detector correlated in space and time. Another possible explanation for multiple ion impacts could be field evaporation of complex ions and their dissociation in the electric field of the APT specimen.[20,21] Closely adjacent detector impact sites of multiples are difficult to resolve and too many detector hits may exceed the detector dead time, leading to a loss of specific atomic species. In the current measurement, 19.8% of the detector hits were multiple events with following contributions: 1.2% N, 9.4% N_2, 0.1% N_3, 0.15% N_2H, 0.2% GaN, 0.03% GaN_3, 8.6% Ga, and 0.1% In. Considering that the majority of N evaporates as molecules, the loss of N due to multiple hits and detector saturation is expected to be higher than for Ga.

An image of the reconstructed specimen is shown in Fig. 5(a). The InGaN layers QW1-QW4 were completely detected while the fifth layer was only partially detected. From the reconstruction, a concentration profile (see Fig. 5(c)) was extracted using a data binning of 0.1 nm. For comparison with the STEM-data, only the In and Ga atoms were

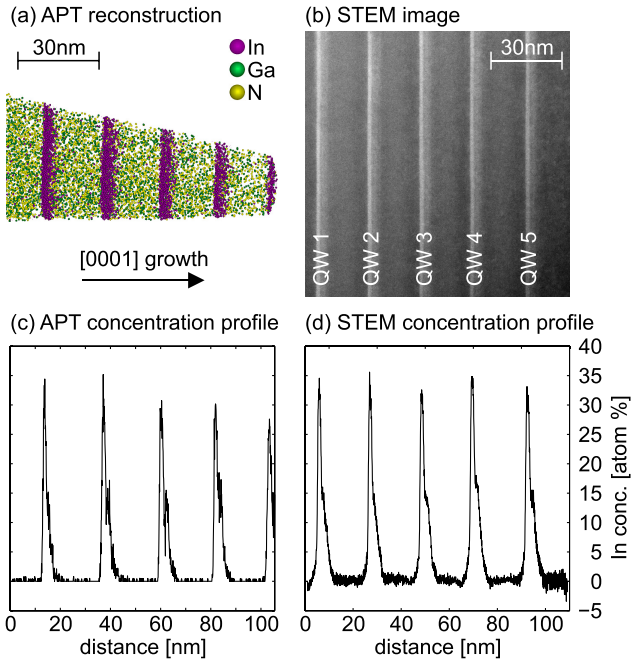

FIG. 5. Atom probe tomography reconstruction (a), HAADF-STEM micrograph (b), concentration profile extracted from APT reconstruction (c), and concentration profile extracted from HAADF-STEM image (d).

taken into account. At the center of the InGaN layer, average In concentrations ranging from 26.2 at. % (QW5) to 31.4 at. % (QW1) have been measured. The values are also listed in Table I. On top of each quantum well, a diffusion layer is visible. Here, concentrations of around 13 at. % In have been measured. Fig. 5(b) depicts an HAADF-STEM overview of the specimen. The image was processed as described above to determine the concentration profile shown in Fig. 5(d). The evaluated concentrations at the center of the quantum wells are also listed in Table I and are ranging from 30.6 at. % (QW5) to 33.4 at. % In measured at QW4. At the diffusion layer on top of the quantum wells, an average In concentration of 14 at. % is measured. A comparison between the concentrations derived by APT and HAADF-STEM (see Table I) reveals a good agreement. Except for QW4 and QW5, the difference is below 2 at. % In. The difference in concentration for QW2 and QW4 can be explained by the fact that the APT and STEM specimens were prepared from different pieces of the sample. Thus, differences in measured concentrations may be due to concentration fluctuations within the wafer.

In conclusion, we demonstrated measurement of specimen thickness and concentrations from HAADF-STEM images for an InGaN sample with high In content by comparison with multislice calculations. Concentrations between 30.6 at. % and 33.4 at. % In have been measured at the center of the InGaN layers and of around 14 at. % at the diffusion

TABLE I. Average In concentration [at. %] measured at the center of the five layers (QW1-5) measured by APT and STEM.

	QW1	QW2	QW3	QW4	QW5
APT	31.4	31.0	29.4	30.2	26.2
STEM	32.1	31.2	31.1	33.4	30.6

layers on top of the quantum wells. The concentrations measured at the quantum well as well as at the diffusion layer are in accordance with concentrations obtained by an alternative atom probe tomography study.

This work was supported by the Deutsche Forschungsgemeinschaft under Contract No. RO2057/8-1 and the Bundesministerium für Bildung und Forschung (BMBF) in the frame of the "ERA-SPOT True Green (13N9634)" project.

[1]I. Vurgaftman, J. R. Meyer, and L. R. Ram-Mohan, J. Appl. Phys. **89**, 5815 (2001).
[2]T. Matsuoka, H. Okamoto, M. Nakao, H. Harima, and E. Kurimoto, Appl. Phys. Lett. **81**, 1246 (2002).
[3]A. Avramescu, T. Lermer, J. Müller, C. Eichler, G. Bruederl, M. Sabathil, S. Lutgen, and U. Strauss, Appl. Phys. Express **3**, 061003 (2010).
[4]A. Rosenauer, W. Oberst, D. Litvinov, D. Gerthsen, A. Förster, and R. Schmidt, Phys. Rev. B **61**, 8276 (2000).
[5]T. M. Smeeton, M. J. Kappers, J. S. Barnard, M. E. Vickers, and C. J. Humphreys, Appl. Phys. Lett. **83**, 5419 (2003).
[6]A. Rosenauer, T. Mehrtens, K. Müller, K. Gries, M. Schowalter, P. Venkata Satyam, S. Bley, C. Tessarek, D. Hommel, K. Sebald, M. Seyfried, J. Gutowski, A. Avramescu, K. Engl, and S. Lutgen, Ultramicroscopy **111**, 1316 (2011).
[7]A. Rosenauer, K. Gries, K. Müller, A. Pretorius, M. Schowalter, A. Avramescu, K. Engl, and S. Lutgen, Ultramicroscopy **109**, 1171 (2009).
[8]L. Hoffmann, H. Bremers, H. Jönen, U. Rossow, M. Schowalter, T. Mehrtens, A. Rosenauer, and A. Hangleiter, Appl. Phys. Lett. **102**, 102110 (2013).
[9]L. Giannuzzi and F. Stevie, Micron **30**, 197 (1999).
[10]T. Mehrtens, S. Bley, P. V. Satyam, and A. Rosenauer, Micron **43**, 902 (2012).
[11]K. Thompson, D. Lawrence, D. Larson, J. Olson, T. Kelly, and B. Gorman, Ultramicroscopy **107**, 131 (2007).
[12]A. Rosenauer and M. Schowalter, in *Microscopy of Semiconducting Materials 2007*, edited by A. Cullis and P. Midgley (Springer, The Netherlands, 2008).
[13]V. Grillo, E. Carlino, and F. Glas, Phys. Rev. B **77**, 054103 (2008).
[14]F. H. Stillinger and T. A. Weber, Phys. Rev. B **31**, 5262 (1985).
[15]S. Plimpton, J. Comput. Phys. **117**, 1 (1995).
[16]M. Schowalter, A. Rosenauer, J. T. Titantah, and D. Lamoen, Acta Crystallogr. **A65**, 227 (2009).
[17]J. M. LeBeau and S. Stemmer, Ultramicroscopy **108**, 1653 (2008).
[18]S. Findlay and J. LeBeau, Ultramicroscopy **124**, 52 (2013).
[19]F. De Geuser, B. Gault, A. Bostel, and F. Vurpillot, Surf. Sci. **601**, 536 (2007).
[20]D. Saxey, Ultramicroscopy **111**, 473 (2011).
[21]M. Müller, B. Gault, G. D. W. Smith, and C. R. M. Grovenor, J. Phys.: Conf. Ser. **326**, 012031 (2011).
[22]See supplementary material at http://dx.doi.org/10.1063/1.4799382 for a parameterization of the simulated reference data of Fig. 3a) for reproduction.